Dynamic behavior and complexity of modulated optical micro ring resonator

Lei Yang (杨 磊)*, Wei Pan (潘 炜), Bin Luo (罗 斌), ShuiYing Xiang (项水英), and Ning Jiang (江 宁)

Center for Information Photonics and Communications, School of Information Science and Technology, Southwest Jiaotong University, Chengdu 610031, China

**Corresponding author: yanglei19811212@sohu.com*

Received November 3, 2010; accepted January 28, 2011; posted online May 6, 2011

The dynamic behavior of an optical micro ring resonator (OMRR) with an amplitude modulator positioned in the micro ring is investigated quantitatively by adopting a recently introduced quantifier, the permutation entropy (PE). The effects of modulation depth are focused on, and the roles of input power are considered. The two-dimensional (2D) maps of PE showing dependence on both modulation depth and input power are presented as well. PE values nearly increase with modulation depth. On the other hand, the optimal value of input power is achieved when the PE reaches its maximum. Thus, PE can successfully quantify the dynamics of modulated OMRR. Selecting the parameters in the region with high PE values would contribute to the complexity-enhanced OMRR-based chaotic communication systems.

OCIS codes: 140.4780, 190.3100, 190.4370.

doi: 10.3788/COL201109.061402.

Optical micro ring resonators (OMRR) attracted considerable attention due to the variety of possible operating regimes[1,2]. These interesting behaviors originated physically from the optical Kerr effect[3]. Since then, a great deal of interest has been concentrated on the OMRR due to its potential applications in secure communication, temperature and pressure sensing, etc.[4−7] Mimuro *et al*. proposed a novel method for measuring the non-linear refractive index using a modulated optical fiber ring resonator, including phase-modulation[8,9]. The output power fluctuated periodically in low input range and exhibited a quasi-periodic fluctuation with increasing input power. Finally, it became chaotic at higher power input. Since the output of resonator is significantly affected by the added modulator, we considered the amplitude-modulated (AM) OMRR and evaluated quantitatively its dynamic behavior.

Recently, several effective tools have been proposed to quantify the complexity of time series, such as the Lyapunov exponents (LE), Kaplan-Yorke dimension, and Kolmogorov-Sinai entropy[10,11]. Likewise, the permutation entropy (PE) proposed has been adopted to quantify the complexity of chaotic signals[12]. Among these quantifiers, PE method can be used for any type of time series. This method has exhibited numerous advantages, such as simplicity, fast calculation process, robustness to noise, and invariance with respect to nonlinear monotonous transformations[13−15]. Moreover, PE-based method has been shown to be 100 times faster than LE-based method[16]. With these advantages, PE was adopted as the dynamic quantifier in this letter. To the best of our knowledge, the study on the complexity of chaotic signals generated by modulated-OMRR using the PE method has not yet been reported.

Recently, our research groups reported successful adoption of PE as a tool to quantify the dynamics of time-delayed erbium-doped fiber dual-ring laser[17]. The PE has also been used to quantify the chaotic complexity of vertical-cavity surface-emitting lasers with polarized optical feedback[18,19]. In the present study, we focused on the dynamic behavior of an amplitude-modulated OMRR.

The schematic of the OMRR used in our simulation is shown in Fig. 1. This is composed of a short piece of optical fiber and an optical fiber coupler (cross-coupled connection). The light circulated in the ring is amplitude-modulated. We assumed that the directional coupler can be characterized by the intensity coupling coefficient κ and fractional coupler intensity loss ρ. Thus, the resonator output field $E_{\rm out}(t)$ consisted of transmitted and circulated components, and expressed as

$$E_{\rm t}(t) = {\rm j}\sqrt{(1-\rho)\kappa}E_{\rm in}(t) + \sqrt{(1-\rho)(1-\kappa)}E_{\rm p}(t), \quad (1)$$

$$E_{\rm out}(t) = {\rm j}\sqrt{(1-\rho)\kappa}E_{\rm p}(t) + \sqrt{(1-\rho)(1-\kappa)}E_{\rm in}(t), \quad (2)$$

where $E_{\rm t}(t)$ and $E_{\rm p}(t)$ are transmitted and circulated optical fields in resonator, respectively, $E_{\rm in}(t)$ is the input optical field, and j is imaginary unit. Relationship between $E_{\rm t}(t)$ and $E_{\rm p}(t)$ in the stationary regime can be obtained from

$$\frac{\partial E}{\partial z} = {\rm j}\frac{2\pi n_2}{\lambda}|E|^2 E - \frac{1}{2}\alpha E. \quad (3)$$

Integrating Eq. (3), we obtain

$$E_{\rm p}(t) = E_{\rm t}(t-\tau_{\rm r})\exp(-\alpha L/2)\exp\left[-{\rm j}\phi(t-\tau_{\rm r})\right], \quad (4)$$

$$\phi(t) = \phi_{\rm L} + \phi_{\rm NL}(t) = \phi_{\rm L} + kn_2 L\left|E_{\rm t}(t)\right|^2, \quad (5)$$

where α and $L = 2\pi R$ are loss coefficient of optical power and the length of the micro ring, respectively, R is the radius of micro ring resonator, $\tau_{\rm r} = n_0 L/c$ is one round-trip time inside the micro ring, $\phi_{\rm L} = kLn_0$ is a linear phase shift, $k = 2\pi/\lambda$ is the wave number of input light in vacuum, and n_0 and n_2 are the core refractive index and the nonlinear refractive index coefficients of the optical micro ring, respectively.

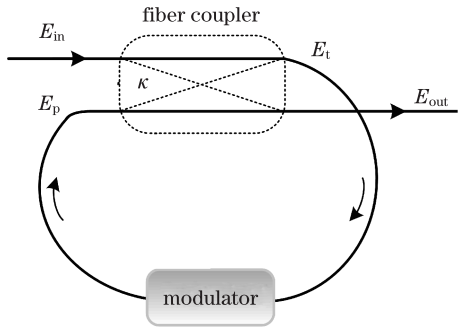

Fig. 1. Schematic of micro ring resonator with a directional coupler (cross-coupled connection) under modulation.

When circulated light is amplitude- or phase-modulated, the output light from Eq. (4) is rewritten as

$$E_{\rm p}(t) = E_{\rm t}(t-\tau_{\rm r})\exp(-\alpha L/2)\exp\big[-{\rm j}(\phi_{\rm L}+kn_2L \big|E_{\rm t}(t-\tau_{\rm r})\big|^2)\big]\times[1+a\cos(2\pi f_{\rm m}t)], \quad (6)$$

$$E_{\rm p}(t) = E_{\rm t}(t-\tau_{\rm r})\exp(-\alpha L/2)\exp\big[-{\rm j}[\phi_{\rm L}+kn_2L \big|E_{\rm t}(t-\tau_{\rm r})\big|^2+m\cos(2\pi f_{\rm m}t)]\big], \quad (7)$$

where m and a are the modulation index and the modulation depth, respectively, and $f_{\rm m}$ is the modulation frequency. In the following simulation, the OMRR output power was normalized, according to

$$P_{\rm out}(t) = |E_{\rm out}(t)|^2/|E_{\rm in}(t)|^2. \quad (8)$$

To evaluate the probability distribution P associated to the time series, we followed the methodology proposed by Bandt *et al.*[16] Partitions of a D-dimensional space that will hopefully reveal relevant details of the ordinal-structure of a given one-dimensional (1D) time series were considered[16−18].

To illustrate the idea, we set a time series $\{x_t, t = 1,\cdots,T\}$, an embedding dimension $D > 1$, and embedding delay $\tau = 1$. "Ordinal patterns" of order D generated by $(s) \mapsto (x_{s-(D-1)}, x_{s-(D-2)},\cdots,x_{s-1},x_s)$ assigns to each time s the D-dimensional vector of values at times $s, s-1,\cdots,s-(D-1)$. The "ordinal pattern" related to the time s refers to the permutation $\pi = (r_0, r_1,\cdots,r_{D-1})$ of $(0,1,\cdots,D-1)$ defined by $x_{s-r_{D-1}} \leqslant x_{s-r_{D-2}} \leqslant \cdots \leqslant x_{s-r_1} \leqslant x_{s-r_0}$. In order to obtain a unique result, we set $r_i < r_{i-1}$ if $x_{s-r_i} = x_{s-r_{i-1}}$. Thus, for all the $D!$ possible permutations π of order D, the probability distribution $P = \{p(\pi)\}$ is defined by[16]

$$p(\pi) = \frac{\#\{s|s\leqslant T-D+1; (x_{s-(D-1)}, x_{s-(D-2)},\cdots,x_{s-1},x_s), \text{has type } \pi\}}{T-D+1}, \quad (9)$$

where the symbol # stands for "number". The PE for the time series $\{x_t, t = 1,\cdots,T\}$ is defined as Shannon entropy:

$$H(P) = -\sum p(\pi)\log p(\pi), \quad (10)$$

where the sum runs over all $D!$ permutation π of order D. For convenience, we further introduced the normalized Shannon entropy $H_{\rm S}[p]$ by[20]

$$H_{\rm S}[p] = H(P)/H_{\max}(0 \leqslant H_{\rm S} \leqslant 1), \quad (11)$$

where $H_{\max} = H[P_{\rm e}] = \log D!$, $P_{\rm e} = \{1/D!,\cdots,1/D!\}$, which means that all $D!$ possible permutations appear with the same probability. In particular, Bandt *et al.* suggested working with $3 \leqslant D \leqslant 7$ for practical purposes, and this is what we adhered to; we chose $D = 5$ and $T = 1000$.

The input light component to the micro ring is given by $E_{\rm in}(t) = E_0\exp({\rm j}\omega t)$, where E_0 and ω are the optical field amplitude and frequency of the pump input light, respectively. The parameters used in our simulation are $\lambda = 1550$ nm, $n_0 = 3.32$, $n_2 = 2.7\times10^{-13}$ m^2/W, $\alpha = 2$ dB/mm, $A_{\rm eff}$=25 μm^2, and the chosen radius of micro ring resonator is R=5 μm. The coupling coefficient and fractional coupler intensity loss of the OMRR were fixed at $\kappa = 0.1$ and $\rho = 0.1$, respectively, and the modulation frequency was set as $f_{\rm m}$=5 kHz. We assumed that $\phi_{\rm L} = 0$ for simplicity.

Bifurcation diagrams and PE as function of the modulation depth for OMRR with $P_{\rm in}$=25 mW are shown in Fig. 2. In Fig. 2(a), the OMRR undergoes several instabilities when the modulation depth increases. The output power periodically fluctuates in low modulation depth range and subsequently exhibits a doubling-periodic fluctuation. Subsequently, the power is routed to chaos for relatively larger modulation depth.

To evaluate the effects of the modulation depth quantitatively, we present PE as further a function of modulation depth in Fig. 2(b). The value of $H_{\rm S}$ is observed as 0 for the 1-periodic state and increases to a relatively high constant level for the 2-periodic state. For multi-periodic states, higher PE values are observed with more cycles. In chaotic regimes, the values of $H_{\rm S}$ fluctuate around a high value, which are significantly larger than those of periodic states. Thus, PE can successfully quantify the dynamics of modulated OMRR. PE agrees well with bifurcation diagrams.

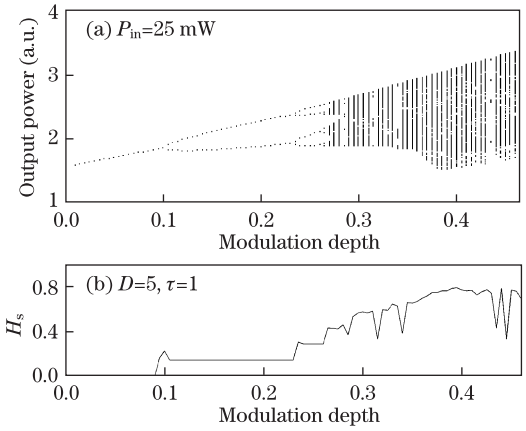

Fig. 2. Bifurcation diagrams and PE as function of the modulation depth with $P_{\rm in}$=25 mW.

The case of OMRR with $a = 0.3$ is taken. The roles of input power are discussed in Fig. 3. The bifurcation diagram as a function of the input power is shown in Fig. 3(a). The OMRR exhibits doubling-periodic fluctuation and subsequently routed to chaos as the input power increases. Interestingly, further increase of input power led to a reverse trend, i.e., from chaos to periodic states. Correspondingly, PE as a function of input power is presented in Fig. 3(b). PE shows obvious increase with the input power, and reaches its maximum at a critical value of input power $P_{\rm in}$=25.2 mW. Subsequently, with the further increase of input power, PE decreases. Thus, increasing the input power beyond the critical value will not yield a higher degree of complexity.

To show the dynamics of OMRR with different modulation depths better, we present the outcomes in time domain in Fig. 4. Four representative cases shown in Fig. 2 are considered. For the case without modulation (i.e., $a = 0$), OMRR behaves as 1-periodic state. On the other hand, when a modulator is included in the micro ring, rich dynamics are observed. When the modulation depth is small, the OMRR still exhibits periodic state behavior. The 1-periodic state is observed for $a = 0.08$ in Fig. 4(b), and 2-periodic state is observed for $a = 0.18$ in Fig. 4(c). For relatively large modulation depth, the chaotic dynamics are rendered for $a = 0.3$ as shown in Fig. 4(d).

In Fig. 5, the two-dimensional (2D) maps of PE showing dependence on both modulation depth and input power are presented. We highlighted the region with high degree of complexity, labeled HH with dashed line H=0.65. Figure 5 shows that the PE values are low for small modulation depths, and the OMRR shows behavior related to periodic state. Moreover, the region HH locates at the middle of the upper side in the parameter space, with large modulation depths and intermediate input power. For the large modulation depth, increasing input power beyond the critical value will not yield a higher degree of complexity. Thus, when using the OMRR as a chaotic carrier, the degree of complexity can be significantly enhanced by properly selecting the input power and the modulation depth according to the 2D maps of PE. This is extremely interesting for OMRR-based chaotic communication systems. We also considered the case of phase-modulated OMRR. Similar results were obtained, which however are not presented.

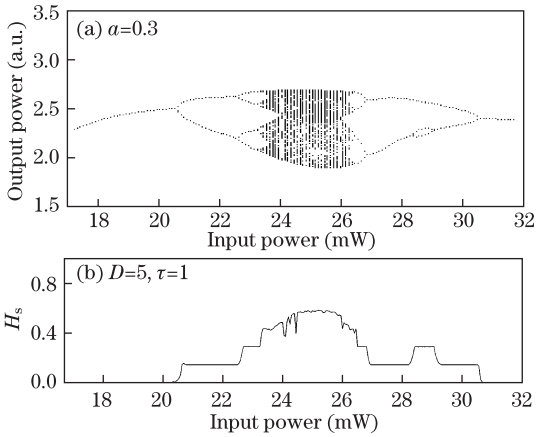

Fig. 3. Bifurcation diagrams and PE as function of the input power with $a = 0.3$.

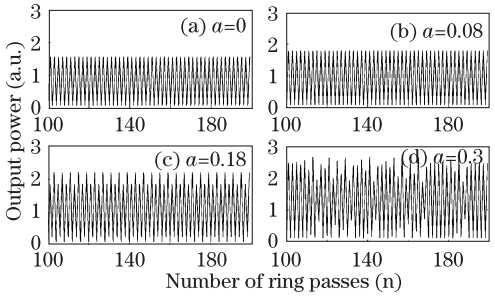

Fig. 4. Typical time traces of modulated OMRR output power with $P_{\rm in}$=25 mW; (a) periodic state without any modulation, (b) 1-period for $a = 0.08$, (c) 2-period for $a = 0.18$, and (d) chaotic state for $a = 0.3$.

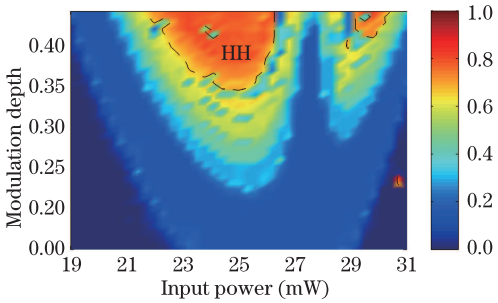

Fig. 5. 2D maps of PE in the parameter space of input power and modulation depth.

In conclusion, we investigate numerically the dynamic behavior of an OMRR with an amplitude modulator setting in the ring. The dynamics of the OMRR are quantified by PE. The trend of PE agrees well with the bifurcation diagrams. In concrete terms, PE values increase with the modulation depth, but the optimal value of input power exists when the PE approaches its maximum. The 2D maps of PE further show that the region HH with high PE values is located at the region with large modulation depths and intermediate input power. This means that for the large modulation depth, increasing the input power beyond the critical value does not yield a higher degree of complexity. Thus, PE can be regarded as an effective tool to quantify the dynamics of modulated OMRR. Selecting the parameters in the region HH according to the 2D maps enhances significantly the complexity and contributes highly to the OMRR-based optical chaotic communication systems.

This work was supported by the National Natural Science Foundation of China (No. 60976039) and the Specialized Research Fund for the Doctoral Program of Higher Education of China (No. 20070613058).

References

1. K. Ogusu, H. Shigekuni, and Y. Yokota, Opt. Lett. **20,** 2288 (1995).
2. K. Ogusu, IEEE J. Quantum Electron. **32,** 1537 (1996).
3. K. Ikeda, H. Daido, and O. Akimoto, Phys. Rev. Lett. **45,** 709 (1980).
4. P. P. Yupapin and W. Suwancharoen, Opt. Commun. **280,** 343 (2007).

5. Y. Imai, S. Yamauchi, H. Yokota, T. Suzuki, and K. Tsuji, Opt. Commun. **282,** 4141 (2009).
6. G. Genty, M. Lehtonen, and H. Ludvigsen, Appl. Phys. B **81,** 357 (2005).
7. F. H. Suhailin, J. Ali, P. P. Yupapin, Y. Fujii, H. Ahmad, and S. W. Harun, Chin. Opt. Lett. **7,** 778 (2009).
8. M. Mimuro, S. Yamauchi, K. Suzuki, and Y. Imai, Opt. Commun. **281,** 469 (2008).
9. T. Suzuki, S. Wei, and Y. Imai, Opt. Rev. **17,** 327 (2010).
10. R. Vicente, J. Daudén, P. Colet, and R. Toral, IEEE J. Quantum Electron. **41,** 541 (2005).
11. D. M. Kane, J. P. Toomey, M. W. Lee, and K. A. Shore, Opt. Lett. **31,** 20 (2006).
12. C. Bandt and B. Pompe, Phys. Rev. Lett. **88,** 174102 (2002).
13. B. Frank, B. Pompe, U. Schneider, and D. Hoyer, Med. Biol. Eng. Comput. **44,** 179 (2006).
14. L. Zunino, D. G. Pérez, M. T. Martín, M. Garavaglia, A. Plastino, and O. A. Rosso, Phys. Lett. A **372,** 4768 (2008).
15. L. Zunino, M. C. Soriano, I. Fischer, O. A. Rosso, and C. R. Mirasso, Phys. Rev. Lett. **82,** 046212 (2010).
16. Y. Cao, W. Tung, J. Gao, V. A. Protopopescu, and L. M. Hively, Phys. Rev. E **70,** 046217 (2004).
17. L. Yang, W. Pan, B. Luo, N. Jiang, and S. Xiang, J. Optoelectron. Laser (in Chinese) (to be published).
18. S. Xiang, W. Pan, L. Yan, B. Luo, X. Zou, N. Jiang, and K. Wen, IEEE J. Selected Topic in Quantum Electron. (to be published).
19. S. Xiang, W. Pan, L. Yan, B. Luo, X. Zou, N. Jiang, and K. Wen, Opt. Lett. **36,** 3 (2011).
20. O. A. Rosso, R. Vicente, and C. R. Mirasso, Phys. Lett. A **372,** 1018 (2008).